

# Seismic behavior of steel tube reinforced concrete bridge columns

Tian Tian<sup>a</sup>, Wen-liang Qiu<sup>\*</sup> and Zhe Zhang<sup>b</sup>

School of Civil Engineering, Dalian University of Technology, Dalian, P.R. China

(Received August 31, 2017, Revised April 11, 2018, Accepted April 17, 2018)

**Abstract.** This paper reports an experimental study that was accomplished to assess the seismic behavior of steel tube reinforced concrete bridge columns (SBCs). The motivation of this study was to verify a supposition that the core steel tube may be terminated at a rational position in the column to minimize the material cost while maintaining the seismic behavior of this composite column. Four SBC specimens were tested under combined constant axial load and cyclic reversed lateral loads. The unique variable in the test matrix was the core steel tube embedment length, which ranged from 1/3 to 3/3 of the column effective height. It is observed that SBCs showed two distinctly different failure patterns, namely brittle shear failure and ductile flexural failure. Tests results indicate that the hysteretic responses of SBCs were susceptible to the core steel tube embedment length. With the increase of this structural parameter, the lateral strength of SBC was progressively improved; the deformability and ductility, however, exhibited a tendency of first increase and then decrease. It is also found that in addition to maintained the rate of stiffness degradation and cumulative energy dissipation basically unchanged, both the ductility and deformability of SBC were significantly improved when the core steel tube was terminated at the mid-height of the column, and these were the most unexpected benefits accompanied with material cost reduction.

**Keywords:** bridge column; seismic behavior; economy; core steel tube; embedment length; cyclic loading

## 1. Introduction

Steel tube reinforced concrete (STRC) column, which consists of a reinforced concrete column and a pre-embedded core steel tube, has received a great deal of attention in China over the past two decades. Formation of this steel-concrete composite column was inspired by the advantages in structural behaviors of concrete-filled steel tube (CFST) (Kwak *et al.* 2013) and steel reinforced concrete (SRC) members (Lu *et al.* 2014). It is expected that pre-embedding a core steel tube into a RC column would give the member not only the direct benefit of strength enhancement, but also the potential benefit of interactions between the encased steel tube and the surrounding concrete, i.e., while the concrete prevents the steel tube from corrosion and local inward/outward buckling, the steel tube provides consistent confinement to the core concrete. Extensive studies have been conducted on STRC columns to investigate their mechanical properties, and the results have demonstrated their favorable axial/eccentric compressive (Nie *et al.* 2005, Guo *et al.* 2013, Han and An 2014), flexural (An *et al.* 2014), and seismic behavior (Ji *et al.* 2014). Recently, the use of STRC columns is becoming an attractive practical solution in tall buildings, industrial plants and underground engineering.

It is well known that bridge columns with insufficient

ductility and energy dissipation capacity are expected to experience severe damage during a major earthquake (Hsu and Fu 2004, Hashimoto *et al.* 2005). Aimed at improving the damage tolerance and seismic resistance of bridge columns, Qiu *et al.* (2013, 2015) suggested that it can be feasible to take use of STRC columns as an alternative to traditional RC columns for bridge construction in seismic regions. Experimental studies performed by Qiu *et al.* (2015) confirmed that the lateral strength, deformability and energy dissipation capacity of STRC bridge columns (SBCs) were considerably superior to those of the RC counterpart. A numerical simulation of a three-span continuous girder bridge under seismic excitations concluded that the maximum drift demand and the residual drift of the superstructure can be substantially reduced by employing SBCs as the substructure (Qiu *et al.* 2013). The results of relevant studies also verified the exceptional seismic behavior of SBCs (Shim *et al.* 2011). Accordingly, it can be foreseen that SBCs have a promising future of application in regions of moderate-to-high seismicity.

For long-span high-pier girder bridges that crossing deep V-shaped valley or approach structures of large-scale bridge projects that crossing sea-straits, incorporating a core steel tube that run through the full-height of a bridge column could significantly increase the investment of earthquake fortification, which will make this composite system less cost-effective. To achieve a balance between the seismic performance and economy for SBCs, the core steel tube may be terminated at the mid-height of bridge columns. In other words, it is merely required to pre-embed a core steel tube into the lower portion of a bridge column. This notion is reasonable because of the fact that bridge columns dissipate earthquake energy primarily depending

\*Corresponding author, Professor,  
E-mail: [qwl@dlut.edu.cn](mailto:qwl@dlut.edu.cn)

<sup>a</sup> Ph.D. Student, E-mail: [tian3316625@163.com](mailto:tian3316625@163.com)

<sup>b</sup> Professor, E-mail: [zhangzhe@dlut.edu.cn](mailto:zhangzhe@dlut.edu.cn)

on the inelastic rotation of their plastic hinges, and simultaneously, the plastic hinge is always the most severely damaged region; therefore, it is only need to reinforce the plastic hinge region so as to enhance its damage resistance and rotational capacity. However, seismic behavior of SBCs that contain core steel tube only in the lower-to-middle portion of the column has not been investigated heretofore and hence test data that can be used to support the notion presented above are not available.

This study was thus conducted to establish understandings pertaining to the seismic behavior of SBCs that partially strengthened by a pre-embedded core steel tube. The main objective of this study was to provide test data and references to determine if the core steel tube can be terminated at a reasonable position. To this end, four specimens were tested under simulated seismic loading conditions to explore the effects of core steel tube embedment length on column behavior. Damage progression and failure modes of the specimens are first described, followed by a detailed discussion on their relative performance based on the recorded hysteretic

## 2. Experimental program

### 2.1 Specimen design and material properties

Four circular bridge column specimens designed in accordance with the guidelines for seismic design of highway bridges (China 2008) were tested under constant axial load and cyclic reversed lateral loads. Table 1 summarizes the structural parameters for each specimen. The unique variable in this test matrix was the core steel tube embedment length,  $l$ , that respectively equal to 1/3, 1/2, 2/3, and 3/3 of the column effective height. The axial load ratio  $n$  was defined as  $n = N/N_0$ , where  $N$  is the axial load applied on the columns, and  $N_0$  is the nominal axially compressive capacity of the column, defined as the product of the gross area of column section and the compressive strength of concrete cylinder. The axial load ratio adopted in this test is typical for actual bridge columns (Ibrahim *et al.* 2016), with the corresponding axial load of 284 kN.

All specimens had the same dimensions and reinforcement details as shown in Fig. 1. Each column was designed

Table 1 Summary of specimen parameters

Specimen	$l$ / mm	$\rho_t$ / %	$\rho_v$ / %	$\rho_t$ / %	$n$	$\lambda$
SBC1	300	1.74	0.84	1.28	0.15	3.0
SBC2	450	1.74	0.84	1.28	0.15	3.0
SBC3	600	1.74	0.84	1.28	0.15	3.0
SBC4	900	1.74	0.84	1.28	0.15	3.0

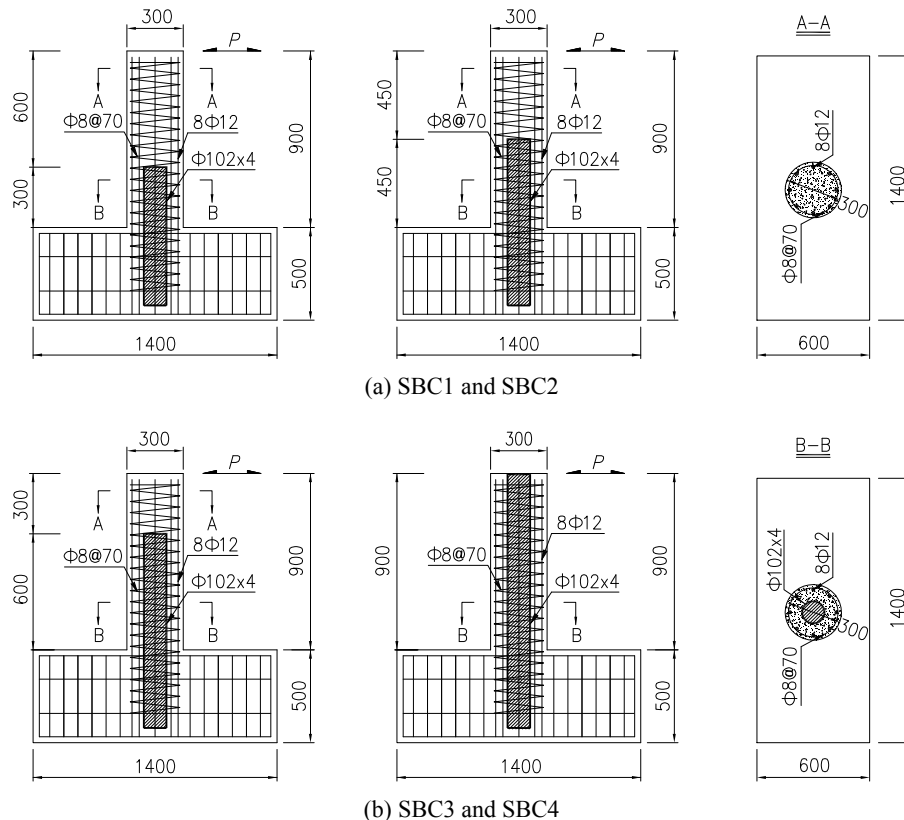


Fig. 1 Dimensions and reinforcements layout of specimens (unit: mm)

to have a effective height of 900 mm with a diameter of 300 mm, which led to a shear span ratio of  $\lambda = 3.0$ . Column effective height was taken from the column-footing interface to the application point of lateral load. The longitudinal steel consisted of eight 12 mm diameter deformed bars uniformly distributed around the perimeter of column section, resulting in a longitudinal steel ratio of  $\rho_l = 1.28\%$ . The stirrups was 8 mm diameter plain bars spaced 70 mm on centers, producing a volumetric steel ratio of  $\rho_v = 0.84\%$ . A clear concrete cover of 15 mm was maintained for stirrups. Low carbon alloy seamless steel tubes with a specification of  $\Phi 102 \times 4$  mm were used as the core steel tubes, yielding a sectional steel tube ratio of  $\rho_{st} = 1.74\%$ . As shown in Fig. 1, a length of 450 mm was provided for column steel tubes to develop adequate anchorage in RC footings, while the steel tubes were extended into the columns with heights of 300 mm, 450 mm, 600 mm, and 900 mm, respectively, for Specimens SBC1~SBC4. The steel tubes were first cut and machined to the required lengths, and then installed into the prefabricated column and footing steel cages with accuracy alignment.

One batch of commercially available concrete with a specified compressive strength of 40 MPa was used to manufacture the specimens. Several 150 mm cubes were also casted and cured adjacent to the column specimens. The average compressive strength for the cubes was about 41.3 MPa at 28 d and 45.0 MPa on the testing day. The measured yield and ultimate strengths of the 12 mm diameter longitudinal bars were 422 MPa and 605 MPa, respectively. The corresponding values for the 8 mm diameter stirrups were 450 MPa and 550 MPa, respectively. Tensile tests were also conducted on coupons cut from the seamless steel tubes, and the obtained yield and ultimate strengths were 368 MPa and 562 MPa, respectively.

## 2.2 Testing apparatus

The cyclic tests were performed in the structural laboratory of Bridge and Tunnel R&D Base at Dalian University of Technology, PR China. A photo of the test set-up is shown in Fig. 2, in which a cantilever-type of loading configuration was employed. Rigid steel beams and high-strength threaded rods were used to tie the column footing to the laboratory strong floor to simulate a boundary condition of full fixity. The axial load was applied via a 3000 kN self-adaption hydraulic jack attached to a roller system. The lateral displacement excursions were imposed through a 1000kN electro-hydraulic servo actuator with  $\pm 300$  mm allowable stroke. A spherical ball seat and a universal joint were introduced between the columns and the aforementioned two sets of loading device to eliminate any constraints to the rotation of columns top-end.

## 2.3 Loading procedure

The axial load was first applied to the columns, and maintained constantly throughout the test. After the axial load was stably established, the cyclic lateral loading commenced in a displacement-controlled manner. The magnitude of the imposed displacement was initially at 2 mm, and subsequently increased to 4, 8, 12, 24, 36, 48, and



Fig. 2 Photo of test set-up

60 mm, with each displacement level cycled thrice until column failure occurs. Column failure was defined as the point at which either the lateral bearing capacity of the specimen dropped to 80% of its measured maximum lateral load or the specimen was unable to sustain the axial compression. To eliminate the interference of strain rate, the lateral excursions were imposed in a gentle way, with each half-cycle took about 2 to 10 minutes, depending on the target displacement level.

## 2.4 Instrumentation and data acquisition

Each specimen was extensively instrumented to monitor the responses during cyclic loading. To obtain the lateral, flexural and shear deformation of the columns, a total of twenty horizontal, vertical, and inclined string potentiometers were placed along the columns at the heights of 100 mm, 200 mm, 400 mm, and 700 mm, respectively, above the column-footing interface. One linear variable differential transducer was installed against the footing of each specimen to observe the lateral movements. Local responses were measured by the electrical resistance strain gages attached to the longitudinal steel, stirrups and steel tubes at two opposite positions in the loading plane. Global responses referred to the forces and displacements at the lateral loading points were recorded automatically by the calibrated actuator sensors with a sampling frequency of 10 Hz. The strain and deformation data were manually acquired by a wireless static strain testing system.

## 3. Test observations and failure mechanism

The failure pattern for each specimen after testing is shown in Fig. 3, horizontal lines marked on the columns spaced 100 mm. Specimen SBC1, contained a 300mm long core steel tube, suffered extensive concrete spalling and longitudinal bar buckling/rapture within a range of 200~400 mm above the column-footing interface, as evident in Fig. 3(a). At a displacement level of 4 mm, several transverse cracks first occurred at the lower portion of the column. As the displacement level increased, the transverse cracks obliquely extended to the side faces of the column, accompanied by appearance of several new diagonal cracks. When the lateral displacement reached 24

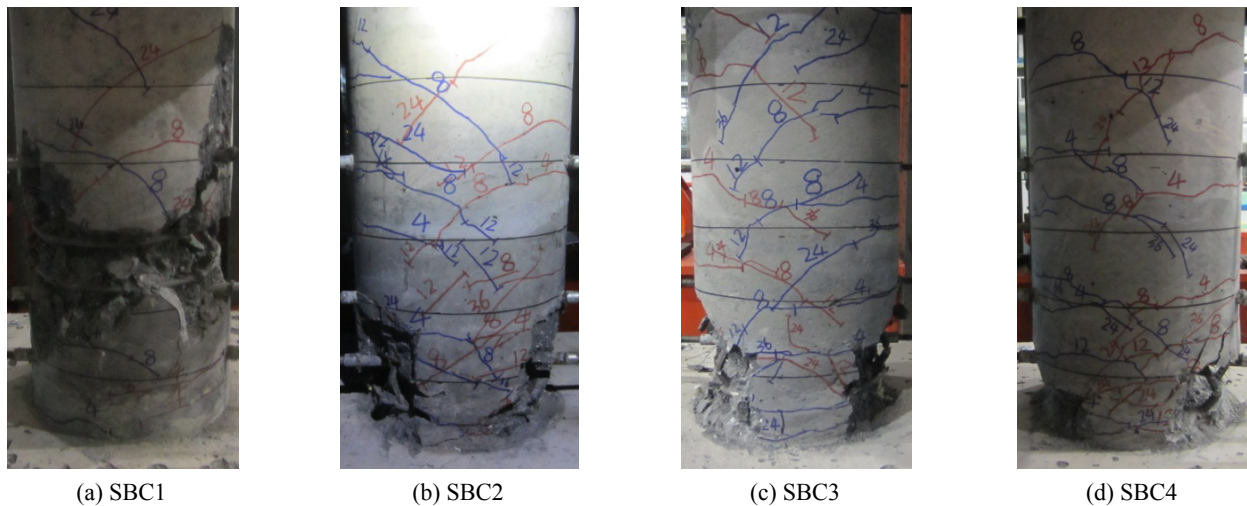


Fig. 3 Failure pattern and crack distribution of specimens

mm, a sudden opening of the transverse and diagonal cracks was observed at the vicinity of the top-end of the core steel tube; these cracks divided the nearby concrete into irregular rhombic debris. Upon further loading, the concrete debris bulged outward and spalled off, while the damaged region extended progressively toward the upper and lower portions of the column. Thereafter, obvious rigid rotation was observed concentrated at the severely damaged zone, which contributed largely to the column lateral displacement. Testing for SBC1 was halted at the conclusion of the first loading cycle to 60 mm displacement level because of dramatic strength deterioration. It should be noted that although this column was failed by severe buckling of longitudinal steel and extensive spalling of concrete, which is an apparent feature of flexural failure, its failure mode was still considered shear failure because of the fully developed inclined cracks and brittle failure process.

Specimens SBC2, SBC3, and SBC4 behaved similarly in damage progression, and all of them suffered ductile flexural failure with most of the visible damage concentrated at the column base. The formation and propagation of initial cracks in these three specimens were identical to those in SBC1 up to 12 mm displacement level. Afterward, almost no new cracks occurred, while several bottom-most transverse cracks developed into critical localized flexural cracks. During the loading cycles to 24 mm displacement level, minor spalling of cover concrete was observed immediately above the column-footing interface. Additional loading cycles beyond this displacement level resulted in substantial crushing of concrete, exposing of steel cage, and buckling/rapture of longitudinal steel bars at both sides of the plastic hinge region. Ultimate failure of these three specimens was reached at the conclusion of 60 mm displacement level. Their failure mode was defined as flexural failure, as evidenced by low-cycle fatigue fracture of longitudinal steel and noticeable degradation of outer concrete within a height of about 200 mm above the column base, as shown in Figs. 3(b)-(d).

Premature termination of the core steel tube was the essential cause for brittle failure of SBC1. During cyclic

loading, the inner CFST column, i.e., consisted of the core steel tube and it encased concrete, was urged to resist the lateral force collaboratively with the outer RC through the pressure imposed by the latter. According to Newton's third law, the outer RC sustained a reaction force provided by the inner CFST. As a matter of fact, the reaction force resulted in a complex stress state in local concrete (nearby the top-end of the core steel tube) which deteriorated the mechanical property of local concrete. When an insufficient embedment length was provided for the core steel tube, which was the case of Specimen SBC1, the inner CFST had a relatively high lateral stiffness, leading to an intense interaction between the two structural components. In this circumstance, the deterioration in mechanical property of local concrete was serious; this caused the damage and rigid rotation localized within the portion of 200 mm~400 mm above the column base. When sufficient embedment lengths were provided for the core steel tube, which were the cases of SBC2 and SBC3, the lateral stiffness of inner CFST was relatively low, while the stress distortion in local concrete and the deterioration to mechanical properties was minor. Compared to the concrete at the column base with higher stress, the damage in the local concrete was lighter, and hence the damage was eventually localized at the column base region to form a flexural plastic hinge, as observed during testing.

## 4. Results and discussion

### 4.1 Hysteretic curves and envelopes

Fig. 4 shows the lateral load versus lateral displacement hysteretic responses of the columns, where the positive and negative stand for the actuator forcing the columns forward and backward, respectively. Specimen SBC1 showed stable hysteretic loops up to a displacement level of 36 mm, after which the cyclic response encountered serious strength degradation. In contrast, Specimens SBC2, SBC3, and SBC4 showed plump hysteretic loops that were stable even after the rupture of longitudinal bars. However, a close

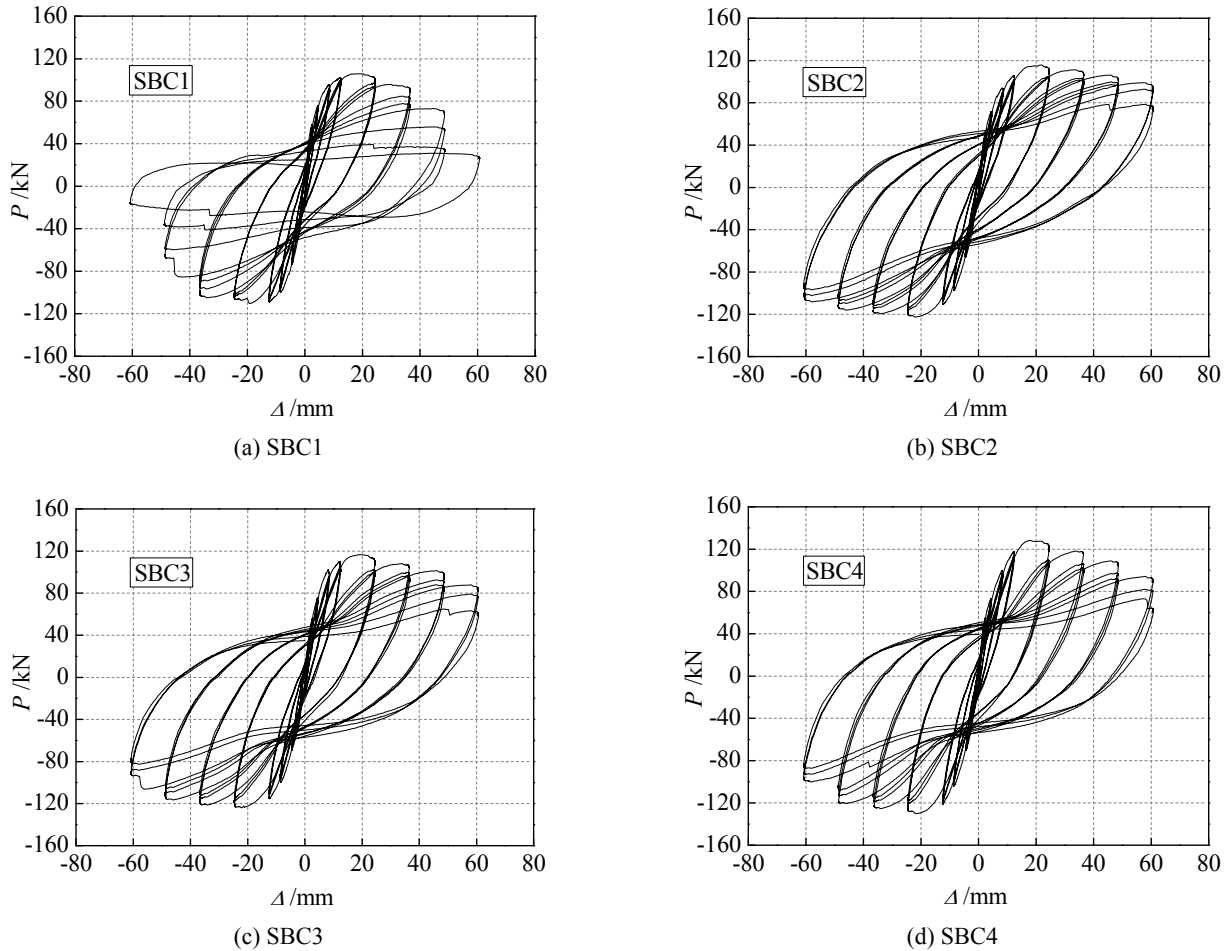


Fig. 4 Load-displacement hysteretic curves

observation between the responses of SBC2, SBC3, and SBC4 reveals that the strength degradation, i.e., the lateral strength decreases with the increasing number of loading cycles under a specific displacement level, in SBC4 was the fastest, and that for SBC2 was the slowest. Specimen SBC3 was in between. This phenomenon is believed to have been caused by the weak bond between the inner CFST and outer RC encasement. Typically, the larger embedment length of the core steel tube, the more spread distribution of the bond cracks, and the faster in column strength degradation. Similar phenomenon can also be found in the research of steel reinforced concrete-reinforced concrete transfer columns (Wu *et al.* 2013, 2016).

The average envelopes of the hysteretic responses in push and pull directions for the tested columns are shown in Fig. 5. No obvious difference was observed between the initial stiffness of the specimens; this indicates that terminating the core steel tube at the column mid-height does not change the free vibration characteristics of bridge structures. Nevertheless, the slope of descending branch in each envelope, which reflected the strength decay after reaching the maximum loading point, was substantially affected by the core steel tube embedment length. Specimen SBC1 showed steep descending branch in its envelope due to rapid progression of physical damage, whereas the descending branch for SBC2 and SBC3 was gentle because

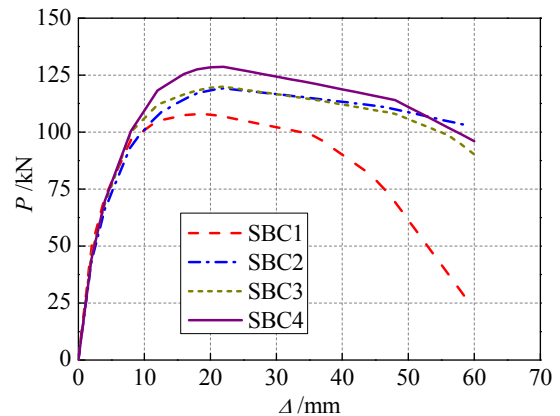


Fig. 5 Comparison of envelopes

both of them failed in a ductile manner. The descending branch of SBC4 was slightly steeper than that of SBC2 and SBC3; this was reasonable and may also be attributed to its more serious bond failure between the inner CFST and outer RC encasement, compared to that of SBC2 and SBC3.

#### 4.2 Measured curvatures

Fig. 6 depicts the curvature distributions of two typical columns at different displacement amplitudes. Curvatures

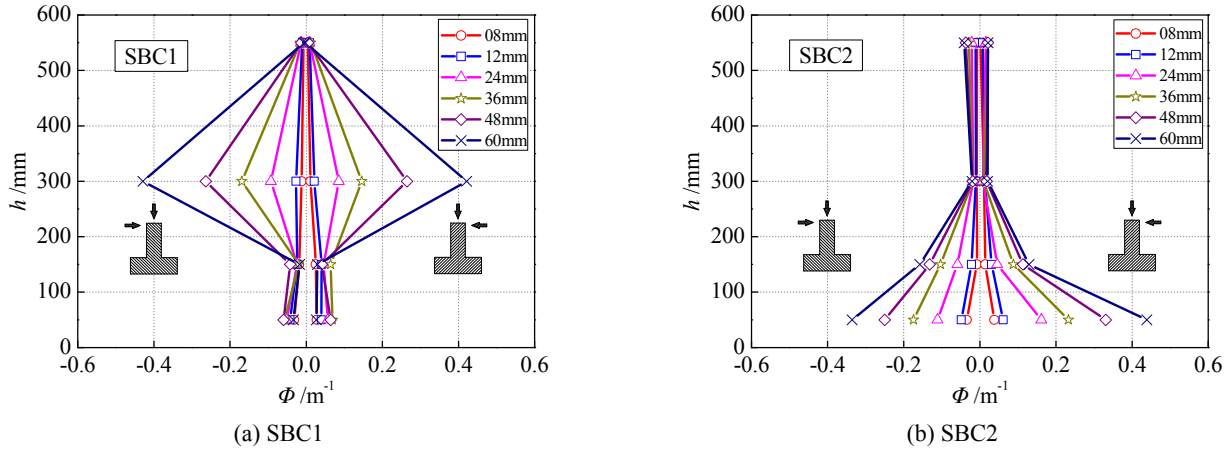


Fig. 6 Curvature distribution of two typical specimens

were obtained from the readings of four pairs of vertical string potentiometers installed along the column height (Saiidi and Tazarv 2016). It is apparent in Fig. 6(a) that the curvature was more localized in the third gauge region (200 mm~400 mm above the column base) for SBC1. This gauge region corresponding to the most damaged area in the column. At a displacement level of 24 mm, a visible increase in curvature was observed in this critical region. After that, displacing the column led to concentrated rotation of this portion, whereas the rotation at the column base basically terminated. It can also be seen that the spacing between the curvature distribution curves of SBC1 increased gradually for the same lateral displacement increment; this indicates that the column experienced an unstable development of rotation at this region. For specimens failed at the column base, taking SBC2 for example, it is clear in Fig. 6(b) that the curvature in the first gauge region (0~100 mm above the column base) exhibited larger values than that of the remainder portions of the column. The curvature curves for SBC2 relating to each displacement level distribute evenly in general; this implies that the rotation developed steadily at the column base region, and the damage progression was smooth and controllable.

#### 4.3 Strength and ductility

Table 2 summarizes the test results at specific points on the envelopes for each specimen, which were obtained by averaging the measurements in the push and pull directions. In Table 2,  $P_y$  and  $\Delta_y$  are the nominal yield load and yield displacement, respectively. The nominal yield displacement  $\Delta_y$  was defined as the displacement of the crossing point of

the following two lines: the straight line that passes through the origin and  $0.75P_m$  of the envelope curve and the line that passes  $P_m$  of the envelope curve parallel to the  $x$ -axis, and the nominal yield load  $P_y$  was defined as the lateral load of the point on the envelope curve corresponding to  $\Delta_y$  (Choi *et al.* 2010);  $P_m$  is the maximum lateral strength;  $\Delta_u$  is the ultimate displacement, defined as the displacement corresponding to the lateral load declined to 85% of the measured maximum strength. The ultimate drift ratio  $\theta_u$  and ductility coefficient  $\mu_\Delta$  used to qualify the deformability and ductility are also included in Table 2. It is generally assumed that  $\theta_u = 5.0\%$  and  $\mu_\Delta = 5.0$  representing a good level of deformability and ductility for bridge columns in engineering practice. As can be obtained from Table 2, the average value of  $\theta_u$  and  $\mu_\Delta$  for the tested specimens were 5.6% and 5.6, respectively. It means that SBCs possess favorable deformability and ductility, and thus have the potential to be utilized in regions of moderate to high seismicity.

One of the main objectives of this study was to understand if the two important seismic measures, i.e., lateral strength and ductility, of SBC would be notably affected by the core steel tube embedment length. Fig. 7 plots the lateral strength against the test variable for the specimens. In general, the lateral strength of SBC increased with the increase of core steel tube embedment length. This was believed to have been caused by the higher flexural stress developed in the core steel tube when a larger embedment length was provided. A core steel tube with higher flexural stress could assist the outer RC encasement to better resist the lateral force, and thereby enhanced the column lateral strength. Fig. 8 shows the ductility versus the test variable for the specimens. As the core steel tube

Table 2 Summary of test results

Specimen	$P_y$ /kN	$\Delta_y$ /mm	$P_m$ /kN	$\Delta_u$ /mm	$\theta_u = \Delta_u/h$	$\mu_\Delta = \Delta_u/\Delta_y$
SBC1	92.78	7.33	108.08	38.98	4.33%	5.32
SBC2	100.09	9.68	119.23	59.91	6.66%	6.19
SBC3	103.72	8.95	120.37	52.68	5.85%	5.88
SBC4	109.37	9.99	128.90	50.24	5.58%	5.03

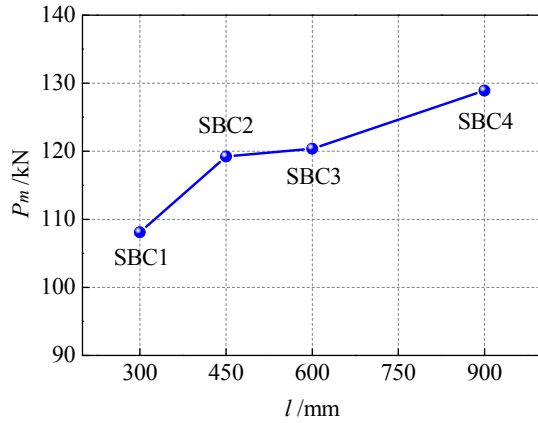


Fig. 7 Comparison of lateral strength

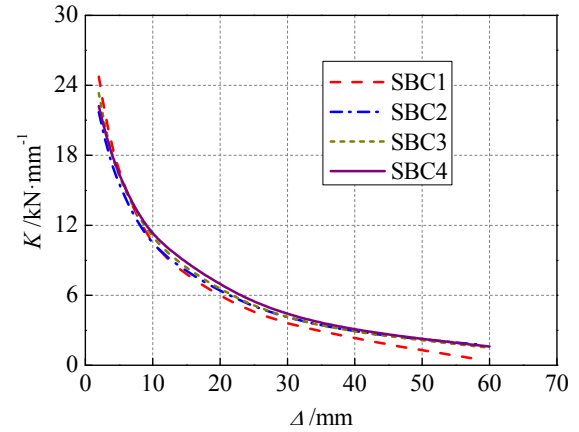


Fig. 9 Comparison of stiffness degradation

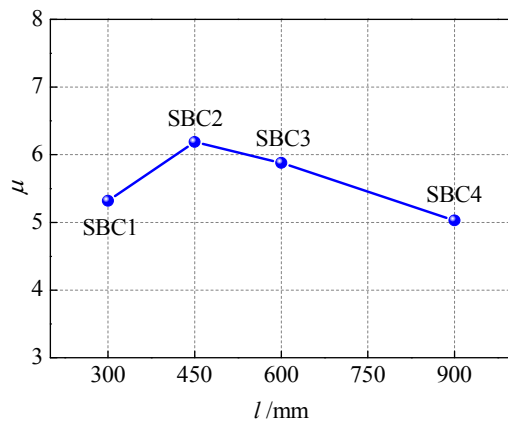


Fig. 8 Comparison of ductility

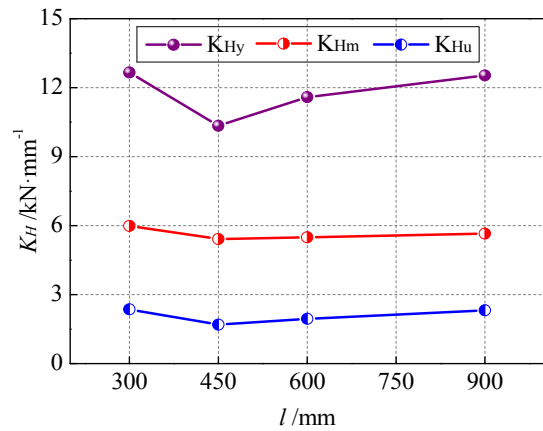


Fig. 10 Comparison of lateral stiffness

embedment length increased from 300 mm to 450 mm, the ductility of SBC improved obviously because of the change of failure mode. As the embedment length continued to increase from 450 mm to 900 mm, the ductility of SBC deteriorated continuously. This is because the bond failure between the inner CFST and outer RC adversely affected the strength degradation under a specific displacement level, which further accelerated the strength decay after reaching the maximum loading point as a chain action.

Compared to SBC4, the lateral strength and ductility of SBC2 were, respectively, lower by 7.5% and higher by 23.1%. This means that the improvement in ductility was about three times the reduction in lateral strength, as the core steel tube embedment length decreased from 900 mm to 450 mm. Considering the philosophy and methodology in current seismic design that the lateral load capacity of a bridge column can be reduced proportionally to its ductility ability, the lower lateral strength in SBC2 is hence not necessarily a concern; because the benefits gained from increased ductility considerably exceeded the disadvantageous effects of column strength reduction on seismic resistance. The higher-than-expected ductility in SBC2 is a sound argument to support the notion previously described that the core steel tube can be terminated at the mid-height of the column.

#### 4.4 Stiffness degradation

Lateral stiffness of bridge columns plays an important role in collapse-resistant for bridge structures. During cyclic loading, secant stiffness defined as the slope of the line connecting the two vertexes in a hysteretic loop is adopted to describe the column lateral stiffness (Choi *et al.* 2013). Fig. 9 shows the lateral stiffness for the specimens as a function of lateral displacement. The lateral stiffness of all four columns followed a similar degradation trend and reduced to around 50% of their initial values at a displacement level of 12 mm. Beyond this displacement level, the lateral stiffness continued to decrease at a lower rate and approached to a constant value at the end of test. SBC1 deteriorated faster in lateral stiffness than other columns because of rapid damage progression. For SBC2, SBC3, and SBC4, which suffered flexure failure at the column base, their stiffness degradation was slower than that of SBC1 and showed no obvious difference over the complete displacement range. Accordingly, it is suggested that the core steel tube can be terminated at the column mid-height provided the column failure mode being not altered.

In previous paragraph, the lateral stiffness of SBC specimens was compared at the same lateral displacement excursions. To further understand the effect of core steel

tube embedment length on column stiffness, Fig. 10 depicts the lateral stiffness versus the test variable for specimens at three characteristic points on each load-displacement envelope. In Fig. 10,  $K_{Hy}$ ,  $K_{Hm}$ , and  $K_{Hu}$  represent column lateral stiffness relating to the yield, maximum, and ultimate points, respectively, and each of them can be obtained by dividing the lateral load by its corresponding lateral displacement. It can be seen in Fig. 10 that the lateral stiffness of SBC generally exhibited a tendency of first decrease and then increase with the increase of core steel tube embedment length. Moreover, the variation of lateral stiffness with the test variable was related to the damage level of the column. Specifically, when the columns suffered a minor damage, the lateral stiffness (i.e.,  $K_{Hy}$ ) was apparently affected by the steel tube embedment length; or vice versa. In addition, a comparison of Figs. 10 and 8 reveals that the lateral stiffness and ductility of SBC generally exhibited the opposite variation tendency with the increasing core steel tube embedment length.

It is well accepted that stiffness degradation generally reflects the cumulative damage in a structural member. In Fig. 10, stiffness degradation of a specimen can be quantitatively evaluated by the difference between the ordinates corresponding to a specific abscissa. As evident in Fig. 10, the difference between  $K_{Hy}$  and  $K_{Hu}$  is the smallest when the abscissa is 450 mm; this implies that SBC2 experienced the slowest stiffness degradation, and hence the most slight physical damage among the four specimens. This may be one of the reasons for SBC2 to sustain its 85% peak strength to a relative large displacement level over other specimens.

#### 4.5 Energy dissipation and residual displacement

Fig. 11 compares the cumulative energy dissipation against the lateral displacement for the specimens. The dissipated energy was determined by integrating the area enclosed by the hysteresis loops (Paultre *et al.* 2009). Fig. 11 illustrates a nonlinear increase in the cumulative energy with the increase of lateral displacement. It can be seen that the energy dissipation was roughly the same for all specimens up to a displacement level of 36 mm. Beyond this displacement level, Specimen SBC1 prematurely failed

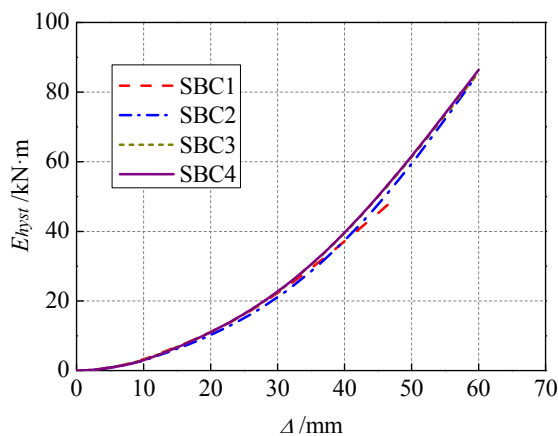


Fig. 11 Comparison of energy dissipation

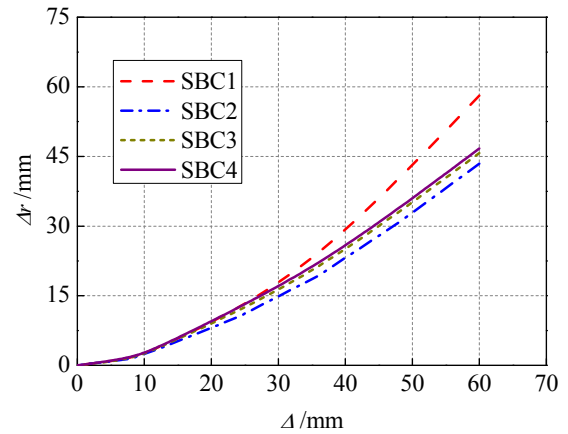


Fig. 12 Comparison of residual displacement

and dissipated less total energy than other three specimens. On the other hand, similar amount of energy was dissipated by SBC2, SBC3 and SBC4 throughout the loading test. This indicates that for SBC dominated by flexural failure, terminating the core steel tube at the column mid-height barely has any detrimental influence on the energy dissipation capacity. Moreover, in view of the fact that the lateral strength of SBC2 and SBC3 was smaller than that of SBC4, it can be inferred that the hysteresis loops of SBC2 and SBC3 were plumper than those of SBC4.

Self-centering capacity is another essential index for seismic assessment. Bridge columns with favorable self-centering capacity could ensure post-earthquake serviceability and reduce repair costs for bridge structures. Self-centering capacity can be evaluated by residual displacement, which defined as displacement at the intersection of the unloading hysteretic curves with the abscissa (Saiidi and Tazarv 2016). Fig. 12 displays the residual displacement at different displacement levels for the tested specimens. As expected, Specimen SBC1 that suffered brittle failure showed the largest residual displacement among the four tested specimens. The residual displacement at 60 mm displacement level for SBC1 was approximately 58 mm; this indicates that SBC1 almost lost its self-centering capacity at this loading cycle. Specimen SBC2, in contrary, exhibited the smallest residual displacement of about 43 mm at 60 mm displacement level. Specimens SBC3 and SBC4 showed practically the same residual displacement in the complete displacement range and was slightly larger than that of SBC2. The results presented in this section clearly demonstrate that the core steel tube can be terminated at the mid-height of the column to facilitate the self-centering capacity while maintaining the energy dissipation capacity.

## 5. Conclusions

An experimental investigation was conducted to provide new knowledge regarding the seismic behavior of SBCs. Effects of core steel tube embedment length were evaluated by testing four geometrically identical specimens under cyclically reversed lateral displacement excitations and constant axial load. Based on the limited results presented

herein, the following observations and conclusions can be made.

Core steel tube embedment length is of an essential structural parameter in determining the failure pattern of SBCs. When a sufficient embedment length is provided for the core steel tube, SBC will subject to ductile flexural failure at the column base; otherwise, brittle shear failure is likely to occur, with the most severely damaged region localized adjacent to the top-end of the core steel tube. Shifting of critical damaged region from column base to column mid-height can be attributed to an increase in the lateral stiffness of the inner CFST column. SBC specimen that experienced shear failure in this testing program exhibited poor deformability, energy dissipation and self-centering capacity, and it also deteriorated faster in lateral stiffness than other three specimens. Consequently, the shear failure of SBC should be strictly prohibited. For SBC specimens suffered flexural failure, the lateral strength was progressively decreased as the core steel tube embedment length decreased from 900 mm to 450 mm. However, the reduction in column lateral strength (7.5%) was inconspicuous and can be negligible, as compared to the significant improvement in deformability (19.4%) and ductility (23.1%). Additionally, there was no obvious difference was observed between their stiffness degradation and cumulative energy dissipation, apart from a mild enhancement in column self-centering capacity was gained as the core steel tube embedment length decreased.

In summary, a comprehensive weighing on the performance of SBCs, from the perspectives of failure mode, lateral strength, deformability, ductility, stiffness degradation, energy dissipation, and self-centering capacity, verified the supposition introduced in this paper that the core steel tube can be terminated at a rational position to reduce the material cost while maintaining the seismic behavior of this composite bridge column.

## Acknowledgments

This research was funded by the National Natural Science Foundation of China (No. 51178080; 51778108). The authors would like to express their sincere appreciation for the financial support.

## References

- An, Y.F., Han, L.H. and Roeder, C. (2014), "Flexural performance of concrete-encased concrete-filled steel tubes", *Mag. Concrete Res.*, **66**(5), 249-267.
- China, C.P. (2008), JTG/T B02-01-2008: Guidelines for seismic design of highway bridges; China Communications Press, Beijing, China. [In Chinese]
- Choi, E., Chung, Y.S., Park, J. and Cho, B.S. (2010), "Behavior of reinforced concrete columns confined by new steel-jacketing method", *ACI Struct. J.*, **107**(6), 654-662.
- Choi, E., Chung, Y.S., Park, C. and Kim, D.J. (2013), "Seismic performance of circular RC columns retrofitted with prefabricated steel wrapping jackets", *Mag. Concrete Res.*, **65**(23), 1429-1440.
- Guo, Q.Q., Zhao, Y.X., Li, Q. and Shang, K. (2013), "Experimental study on eccentric compressive property of steel tube-reinforced concrete columns", *J. Build Struct.*, **34**(12), 103-111. [In Chinese]
- Han, L.H. and An, Y.F. (2014), "Performance of concrete-encased CFST short columns under axial compression", *J. Constr. Steel Res.*, **93**(1), 62-76.
- Hashimoto, S., Fujino, Y. and Abe, M. (2005), "Damage analysis of Hanshin expressway viaducts during 1995 Kobe Earthquake. II: damage mode of single reinforced concrete Piers", *J. Bridge Eng.*, **10**(1), 54-60.
- Hsu, Y.T. and Fu, C.C. (2004), "Seismic effect on highway bridges in Chi Chi Earthquake", *J. Perform. Constr. Fac.*, **18**(1), 47-53.
- Ibrahim, A.M.A., Wu, Z.S., Fahmy, M.F.M. and Kamal, D. (2016), "Experimental study on cyclic response of concrete bridge columns reinforced by steel and basalt FRP reinforcements", *J. Compos. Constr.*, **20**(3), 04015062.
- Ji, X.D., Kang, H.Z., Chen, X.C. and Qian, J.R. (2014), "Seismic behavior and strength capacity of steel tube-reinforced concrete composite columns", *Earthq. Eng. Struct. Dyn.*, **43**(4), 487-505.
- Kwak, J.H., Kwak, H.G. and Kim, J.K. (2013), "Behavior of circular CFT columns subject to axial force and bending moment", *Steel Compos. Struct., Int. J.*, **14**(2), 173-190.
- Lu, X.L., Xue, J.Y., Yin, X.W. and Jiang, H.J. (2014), "Experimental study on hysteretic properties of SRC columns with high steel ratio", *Steel Compos. Struct., Int. J.*, **17**(3), 287-303.
- Nie, J.G., Bai, Y., Li, S.Y., Zhao, J. and Xiao, Y. (2005), "Analyses on composite column with inside concrete filled steel tube under axial compression", *China Civil Eng. J.*, **38**(9), 9-13. [In Chinese]
- Paultre, P., Eid, R., Robles, H.I. and Bouaanani, N. (2009), "Seismic performance of circular high-strength concrete columns", *ACI Struct. J.*, **106**(4), 395-404.
- Qiu, W.L., Jiang, M., Pan, S.S. and Zhang, Z. (2013), "Seismic responses of composite bridge piers with CFT columns embedded inside", *Steel Compos. Struct., Int. J.*, **15**(3), 343-355.
- Qiu, W.L., Kao, C.S., Kou, C.H. and Tasi, J.L. (2015), "Experimental study of seismic performances of RC bridge columns with CFST column embedded inside", *J. Mar. Sci. Tech.*, **23**(2), 212-219.
- Saiedi, M.S. and Tazarv, M. (2016), "Low-damage precast columns for accelerated bridge construction in high seismic zones", *J. Bridge Eng.*, **21**(3), 04015056.
- Shim, C.S., Chung, Y.S. and Yoon, J.Y. (2011), "Cyclic behavior of prefabricated circular composite columns with low steel ratio", *Eng. Struct.*, **33**(9), 2525-2534.
- Wu, K., Xue, J.Y. and Zhao, H.T. (2013), "Failure mechanism and bearing capacity of transfer columns in SRC-RC hybrid structures", *Eur. J. Environ. Civil Eng.*, **17**(S1), 205-228.
- Wu, K., Xue, J.Y., Nan, Y. and Zhao, H.T. (2016), "Experimental research on seismic behavior of SRC-RC transfer columns", *Steel Compos. Struct., Int. J.*, **21**(1), 157-175.

BU